Article:

Wang, J and Yu, H-S (2014) Three-dimensional shakedown solutions for anisotropic cohesive-frictional materials under moving surface loads. International Journal for Numerical and Analytical Methods in Geomechanics, 38 (4). pp. 331-348. ISSN 0363-9061

https://doi.org/10.1002/nag.2207

Three-dimensional shakedown solutions for anisotropic cohesive-frictional materials under moving surface loads

Journal:	*International Journal for Numerical and Analytical Methods in Geomechanics*
Manuscript ID:	NAG-12-0282.R2
Wiley - Manuscript type:	Research Article
Date Submitted by the Author:	n/a
Complete List of Authors:	Wang, Juan; University of Nottingham, Faculty of Engineering yu, hai-sui; University of nottingham, Faculty of Engineering
Keywords:	shakedown analysis, Mohr-Coulomb criterion, cross-anisotropy, plastic anisotropy, moving loads

Three-dimensional shakedown solutions for anisotropic cohesive-frictional materials under moving surface loads

Dr Juan Wang, BEng, MSc, PhD, Research Fellow

and

Professor Hai-Sui Yu, FREng, Pro-Vice-Chancellor and Professor of Geotechnical Engineering (corresponding author)

Email: hai-sui.yu@nottingham.ac.uk

Tel: 0115 823 2487

Address: Nottingham Centre for Geomechanics

Faculty of Engineering

The University of Nottingham

Nottingham, UK

NG7 2RD

Abstract

Previous work on three-dimensional shakedown analysis of cohesive-frictional materials under moving surface loads has been entirely for isotropic materials. As a result, the effects of anisotropy, both elastic and plastic, of soil and pavement materials are ignored. This paper will, for the first time, develop three-dimensional shakedown solutions to allow for the variation of elastic and plastic material properties with direction. Melan's lower-bound shakedown theorem is used to derive shakedown solutions. In particular, a generalised, anisotropic Mohr-Coulomb yield criterion and cross-anisotropic elastic stress fields are utilised to develop anisotropic shakedown solutions. It is found that shakedown solutions for anisotropic materials are dominated by Young's modulus ratio for the cases of subsurface failure and by shear modulus ratio for the cases of surface failure. Plastic anisotropy is mainly controlled by material cohesion ratio, the rise of which increases the shakedown limit until a maximum value is reached. The anisotropic shakedown limit varies with frictional coefficient and the peak value may not occur for the case of normal loading only.

Keywords

Shakedown analysis; Mohr-Coulomb criterion; cross-anisotropy; plastic anisotropy; moving loads

1. Introduction

Shakedown is known as a phenomenon at which an elastic-plastic structure would respond purely elastically to a cyclic load (which is above the yield limit and below a shakedown load limit) after the initial build-up of some plastic deformation. Alternatively, if the load applied is above the shakedown load limit, the structure will finally fail due to fatigue or unlimited incremental plastic deformation or instantaneous collapse [1].

In the field of geotechnical engineering, it has been recognised through experimental and numerical work that shakedown theory has potential applications in solving problems of road pavements under moving traffic loads [2-6]. A key task of applying shakedown theory to pavement design is to determine theoretically the shakedown limit for a given pavement structure. Two fundamental theorems can be used for this purpose: kinematic or upper-bound shakedown theorem [7], and static or lower-bound shakedown theorem [8]. While the upper-bound shakedown theorem has been used for pavement shakedown analysis in consideration of both two-dimensional and three-dimensional surface loads [9-11], the use of lower-bound shakedown theorem was mainly limited to two-dimensional cases [4, 5, 12-16]. The lower bound solutions had not been fully extended to three-dimensional cases until the analytical work of [17-18]. The most recent lower-bound shakedown solutions presented by Yu and Wang [18] were based on an assumption that the cohesive-frictional half-space is isotropic. In reality, however, it has been widely accepted that soils and pavement materials exhibit some degree of anisotropy, because particles deposited vertically tends to be oriented in the horizontal direction [19-21]. And it has been found that ignoring soil anisotropy may result in an overestimation of ultimate bearing capacity and thus lead to an unsafe design [19, 22-24].

1.1. Elastic Anisotropy

For many ground deformation problems, soils are assumed to have a single vertical axis of symmetry with the same properties in any horizontal direction but different properties in the vertical direction [25]. This kind of anisotropy is known as cross-anisotropy or transverse isotropy. In the elastic range, the behaviour of a cross-anisotropic material can be described as follows:

$$\begin{bmatrix} \delta\varepsilon_{xx} \\ \delta\varepsilon_{yy} \\ \delta\varepsilon_{zz} \\ \delta\varepsilon_{xy} \\ \delta\varepsilon_{xz} \\ \delta\varepsilon_{yz} \end{bmatrix} = \begin{bmatrix} 1/E_h & -\upsilon_h/E_h & -\upsilon_{vh}/E_v & & & \\ -\upsilon_h/E_h & 1/E_h & -\upsilon_{vh}/E_v & & & \\ -\upsilon_{hv}/E_h & -\upsilon_{hv}/E_h & 1/E_v & & & \\ & & & 1/2G_h & & \\ & & & & 1/2G_{vh} & \\ & & & & & 1/2G_{vh} \end{bmatrix} \begin{bmatrix} \delta\sigma_{xx} \\ \delta\sigma_{yy} \\ \delta\sigma_{zz} \\ \delta\sigma_{xy} \\ \delta\sigma_{xz} \\ \delta\sigma_{yz} \end{bmatrix}, \qquad (1)$$

where the stress increments $\delta\sigma_{ij}$ and strain increments $\delta\varepsilon_{ij}$ are referred to Cartesian axes (i.e. i and j denote x axis, y axis or z axis), with the z axis being vertical; E_h is Young's modulus in horizontal (H) direction; E_v is Young's modulus in vertical (V) direction; G_h is shear modulus in horizontal plane; G_{vh} is shear modulus in VH plane; υ_h is Poisson's ratio (effect of horizontal strain on complementary horizontal strain); υ_{vh} is Poisson's ratio (effect of vertical strain on horizontal strain); υ_{hv} is Poisson's ratio (effect of horizontal strain on vertical strain).There are two correlations between these parameters (Eq.2 – Eq.3), so that a cross anisotropic material can be fully defined by five independent parameters.

$$G_h = \frac{E_h}{2(1+\upsilon_h)}, \qquad (2)$$

$$\frac{\upsilon_{vh}}{\upsilon_{hv}} = \frac{E_v}{E_h}. \qquad (3)$$

Elastic properties of anisotropic soils have been widely explored. For example, typical values of E_v/E_h for clays may range from 0.25 to 1.11 [25-27]. Experimental results for sands [28, 29] and gravel [30] also show some degree of inherent anisotropy with E_v/E_h from 1.06 to 2. Graham and Houlsby [21] proposed that the elastic anisotropy of natural clays can be described by three parameters: E^* and υ^* and α by giving the following definitions: $E_v = E^*$, $E_h = \alpha^2 E^*$, $\upsilon_h = \upsilon^*$, $\upsilon_{vh} = \upsilon^*/\alpha$, $G_{vh} = \alpha E^*/(2+2\upsilon^*)$, $G_h = \alpha^2 E^*/(2+2\upsilon^*)$.

1.2. Plastic Anisotropy

Laboratory tests performed on soil specimens cut at different orientations have also demonstrated the directional dependence of soil shear strength (eg. [20, 31-33]). It has been shown that the variation of soil cohesion with direction due to inherent anisotropy is much more significant than the effect of anisotropy on the friction angles (eg. [20, 33, 34]). Various failure criterions have also been suggested to describe this anisotropic behaviour of soils (eg. [35, 36]). However these models are usually too sophisticated to be used in practice.

The main purpose of this paper is to develop lower-bound shakedown solutions for anisotropic soils under three-dimensional moving surface loads. Following Yu [17] and Yu and Wang [18], Melan's static shakedown theorem will be used to derive the lower-bound shakedown solutions. Melan's shakedown theorem states that an elastic-perfectly plastic structure will shakedown if the combination of load induced elastic stress field and self-equilibrated residual stress field does not violate the yield criterion. In this paper, a generalised, anisotropic Mohr-Coulomb yield criterion will be utilised, which accounts for the effect of anisotropic cohesion. The elastic anisotropy will also be considered by using elastic stresses in a cross-anisotropic half-space.

2. Problem definition

This paper considers a homogeneous half space of a cohesive-frictional soil that is cross-anisotropic with a vertical axis of symmetry, as shown in Figure 1. As mentioned earlier, the strength anisotropy of soils will also be considered by using a generalized, anisotropic yield criterion. A three-dimensional surface contact load, including a normal pressure p and a surface traction q, moves along x-direction. p and q are assumed to be distributed according to the following equations within a circle of radius a ($x^2+y^2 \le a^2$):

$$p = \frac{3P}{2\pi a^3}\left(a^2 - x^2 - y^2\right)^{1/2}, \tag{4}$$

$$q = \frac{3Q}{2\pi a^3}\left(a^2 - x^2 - y^2\right)^{1/2}, \tag{5}$$

where P is the total normal force in the z-direction and Q is the total shear force in the x-direction. This load distribution is also known as the three-dimensional Hertz load distribution. It has a maximum pressure $p_0 = 3P/2\pi a^2$ at the centre of contact area ($x = y = z = 0$). The normal and shear loads are assumed to be correlated by a frictional coefficient $\mu = Q/P$.

3. Elastic stress field in a cross-anisotropic half space

Hanson [37] derived closed-form expressions for elastic stresses in a cross-anisotropic half space $z > 0$, due to the three-dimensional Hertz load distribution, defined in Eq.4 – Eq.5. Five elastic constants $A_{11}, A_{13}, A_{33}, A_{44}, A_{66}$ were used to define the material behavior as below:

$$\begin{bmatrix} \delta\sigma_{xx} \\ \delta\sigma_{yy} \\ \delta\sigma_{zz} \\ \delta\sigma_{xy} \\ \delta\sigma_{xz} \\ \delta\sigma_{yz} \end{bmatrix} = \begin{bmatrix} A_{11} & A_{11}-2A_{66} & A_{13} & & & \\ A_{11}-2A_{66} & A_{11} & A_{13} & & & \\ A_{13} & A_{13} & A_{33} & & & \\ & & & A_{66} & & \\ & & & & A_{44} & \\ & & & & & A_{44} \end{bmatrix} \begin{bmatrix} \delta\varepsilon_{xx} \\ \delta\varepsilon_{yy} \\ \delta\varepsilon_{zz} \\ \delta\varepsilon_{xy} \\ \delta\varepsilon_{xz} \\ \delta\varepsilon_{yz} \end{bmatrix}. \tag{6}$$

These five constants correlate with Young's modulus, shear modulus and Poisson's ratio as follows: $A_{11} = \frac{1-\upsilon_{vh}\upsilon_{hv}}{E_h E_v \Delta}$, $A_{13} = \frac{\upsilon_{hv}+\upsilon_h\upsilon_{hv}}{E_h^2\Delta}$, $A_{33} = \frac{1-\upsilon_h^2}{E_h^2\Delta}$, $A_{44} = 2G_{vh}$, $A_{66} = 2G_h = \frac{E_h}{1+\upsilon_h}$, where $\Delta = \frac{(1+\upsilon_h)(1-\upsilon_h-2\upsilon_{hv}\upsilon_{vh})}{E_h^2 E_v}$.

Using stress combinations $\sigma_1 = \sigma_{xx} + \sigma_{yy}$, $\sigma_2 = \sigma_{xx} - \sigma_{yy} + 2i\sigma_{xy}$, $\tau_z = \sigma_{xz} + i\sigma_{yz}$, the following elastic stress expressions were given by Hanson [37].

The elastic stresses due to the normal load P are given below:

$$\sigma_1 = \frac{6HPA_{66}}{a^3}\sum_{k=1}^{2}\left\{\frac{\gamma_k^2 - (1+m_k)\gamma_3^2}{\gamma_k(m_k-1)}\left[z_k \arcsin\left(\frac{l_{1k}(a)}{\rho}\right) - \sqrt{a^2 - l_{1k}^2(a)}\right]\right\}, \tag{7}$$

$$\sigma_2 = -\frac{2HPA_{66}}{a^3}\frac{e^{2i\varphi}}{\rho^2}\sum_{k=1}^{2}\left\{\frac{\gamma_k}{(m_k-1)}\left[2a^3 - \left(l_{1k}^2(a) + 2a^2\right)\sqrt{a^2 - l_{1k}^2(a)}\right]\right\}, \tag{8}$$

$$\sigma_z = \frac{3P}{2\pi a^3(\gamma_1-\gamma_2)}\sum_{k=1}^{2}\left\{(-1)^{k+1}\gamma_k\left[z_k \arcsin\left(\frac{l_{1k}(a)}{\rho}\right)-\sqrt{a^2-l_{1k}^2(a)}\right]\right\}, \tag{9}$$

$$\tau_z = \frac{3P}{4\pi a^3(\gamma_1-\gamma_2)}\rho e^{i\varphi}\sum_{k=1}^{2}\left\{(-1)^{k+1}\left[-\arcsin\left(\frac{l_{1k}(a)}{\rho}\right)+\frac{a\sqrt{l_{2k}^2(a)-a^2}}{l_{2k}^2(a)}\right]\right\}. \tag{10}$$

The elastic stresses due to the tangential load Q are given below:

$$\sigma_1 = \frac{3HQA_{66}\gamma_1\gamma_2}{2a^3}\left(e^{i\varphi}+e^{-i\varphi}\right)\rho\sum_{k=1}^{2}\left\{\frac{\gamma_k^2-(1+m_k)\gamma_3^2}{\gamma_k^2(m_k-1)}\left[-\arcsin\left(\frac{l_{1k}(a)}{\rho}\right)+\frac{l_{1k}(a)}{\rho^2}\sqrt{\rho^2-l_{1k}^2(a)}\right]\right\}, \tag{11}$$

$$\begin{aligned}\sigma_2 = {} & \frac{3HQA_{66}\gamma_1\gamma_2}{a^3}\sum_{k=1}^{2}\left\{\frac{1}{(m_k-1)}\left[e^{i\varphi}\left\{\frac{1}{2}\rho\arcsin\left(\frac{l_{1k}(a)}{\rho}\right)-\frac{l_{1k}(a)}{2\rho}\sqrt{\rho^2-l_{1k}^2(a)}\right\}\right.\right.\\ & \left.\left.-e^{i3\varphi}\left\{\frac{4z_k}{3\rho^3}\left(\left[l_{1k}^2(a)+2a^2\right]\sqrt{a^2-l_{1k}^2(a)}-2a^3\right)+\frac{l_{1k}^3(a)}{\rho^3}\sqrt{\rho^2-l_{1k}^2(a)}\right\}\right]\right\}\\ & -\frac{3Q}{2\pi a^3\gamma_3}\left[e^{i\varphi}\left\{\frac{1}{2}\rho\arcsin\left(\frac{l_{13}(a)}{\rho}\right)-\frac{l_{13}(a)}{2\rho}\sqrt{\rho^2-l_{13}^2(a)}\right\}\right.\\ & \left.+e^{i3\varphi}\left\{\frac{4z_3}{3\rho^3}\left(\left[l_{13}^2(a)+2a^2\right]\sqrt{a^2-l_{13}^2(a)}-2a^3\right)+\frac{l_{13}^3(a)}{\rho^3}\sqrt{\rho^2-l_{13}^2(a)}\right\}\right],\end{aligned} \tag{12}$$

$$\sigma_z = \frac{3Q\gamma_1\gamma_2}{8\pi a^3(\gamma_1-\gamma_2)}\left(e^{i\varphi}+e^{-i\varphi}\right)\rho\sum_{k=1}^{2}\left\{(-1)^{k+1}\left[-\arcsin\left(\frac{l_{1k}(a)}{\rho}\right)+\frac{l_{1k}(a)}{\rho^2}\sqrt{\rho^2-l_{1k}^2(a)}\right]\right\}, \tag{13}$$

$$\begin{aligned}\tau_z = {} & \frac{3Q\gamma_1\gamma_2}{4\pi a^3(\gamma_1-\gamma_2)}\sum_{k=1}^{2}\left\{\frac{(-1)^{k+1}}{\gamma_k}\left[-z_k\arcsin\left(\frac{l_{1k}(a)}{\rho}\right)+\sqrt{a^2-l_{1k}^2(a)}-e^{i2\varphi}\frac{2a^3-\left(l_{1k}^2(a)+2a^2\right)\sqrt{a^2-l_{1k}^2(a)}}{3\rho^2}\right]\right\}\\ & -\frac{3Q}{4\pi a^3}\left[-z_3\arcsin\left(\frac{l_{13}(a)}{\rho}\right)+\sqrt{a^2-l_{13}^2(a)}+e^{i2\varphi}\frac{2a^3-\left(l_{13}^2(a)+2a^2\right)\sqrt{a^2-l_{13}^2(a)}}{3\rho^2}\right],\end{aligned} \tag{14}$$

where

$\gamma_k^2 = n_k \ (k=1,2)$,

$\gamma_3^2 = \dfrac{A_{44}}{A_{66}}$,

n_k are the two (real or complex conjugate) roots of the quadratic equation:

$$A_{11}A_{44}n^2+\left[A_{13}\left(A_{13}+2A_{44}\right)-A_{11}A_{33}\right]n+A_{33}A_{44}=0\,,$$

$$H=\frac{\left(\gamma_1+\gamma_2\right)A_{11}}{2\pi\left(A_{11}A_{33}-A_{13}^2\right)}\,,$$

$$z_k=\frac{z}{\gamma_k}\,,$$

$$\rho=\sqrt{x^2+y^2}\,,$$

$$\varphi=\begin{cases}0 & \text{if } y=0\;\&\; x=0\\ \arcsin\left(y/\rho\right) & \text{if } x\geq 0\\ \text{-}\arcsin\left(y/\rho\right)+\pi & \text{if } x<0\end{cases}\,,$$

$$l_{1k}\left(a\right)=\frac{1}{2}\left(\sqrt{\left(\rho+a\right)^2+z_k^2}-\sqrt{\left(\rho-a\right)^2+z_k^2}\right),$$

$$l_{2k}\left(a\right)=\frac{1}{2}\left(\sqrt{\left(\rho+a\right)^2+z_k^2}+\sqrt{\left(\rho-a\right)^2+z_k^2}\right).$$

The elastic stresses that are relevant to this study can be obtained using $\sigma_{xx}=\left[\sigma_1+\text{real}\left(\sigma_2\right)\right]/2$, $\sigma_{xz}=\text{real}(\tau_z)$, $\sigma_{zz}=\text{real}(\sigma_z)$ (the imaginary part of σ_z was found to be very small).

4. Plastic anisotropy

Lo [32] assumed that the directional strength, in particular the variation of cohesion with direction, can be described by the following mathematical expression:

$$c_\theta=c_h+(c_v-c_h)\sin^2\theta\,, \tag{15}$$

where c_h and c_v are the values of cohesion on the horizontal and vertical planes respectively and c_θ represents the cohesion measured on a plane inclined at an angle θ to the horizontal plane.

For an anisotropic material, the conventional isotropic Mohr-Coulomb failure criterion is no longer valid. According to Yu and Sloan [24], if compressive stresses are treated as positive, the shear strength developed on the plane ab (shown in Figure 2) can be found as:

$$s = c_\theta - \sigma_n \tan\phi = c_h + (c_v - c_h)\sin^2\theta - \sigma_n \tan\phi\,, \tag{16}$$

with normal and shear stress components on plane ab:

$$\sigma_n = \sigma_{xx}\sin^2\theta + \sigma_{zz}\cos^2\theta - \sigma_{xz}\sin 2\theta\,, \tag{17}$$

$$\tau = -\sigma_{xx}\sin\theta\cos\theta + \sigma_{zz}\sin\theta\cos\theta + \sigma_{xz}\cos 2\theta\,. \tag{18}$$

where ϕ is material friction angle.

The shear stress must be smaller than the shear strength (i.e. $\tau - s \le 0$), so that:

$$\begin{aligned}&\left[-\sigma_{xx}\sin\theta\cos\theta + \sigma_{zz}\sin\theta\cos\theta + \sigma_{xz}\cos 2\theta\right]\\ &-\left[c_h + \left(c_v - c_h\right)\sin^2\theta - \tan\phi\left(\sigma_{xx}\sin^2\theta + \sigma_{zz}\cos^2\theta - \sigma_{xz}\sin 2\theta\right)\right] \le 0.\end{aligned} \tag{19}$$

Using the following equation for the orientation of the critical plane,

$$\frac{\partial(\tau - s)}{\partial\theta} = 0 \Rightarrow \tan 2\theta = \frac{\sigma_{zz} - \sigma_{xx} - 2\sigma_{xz}\tan\phi}{c_v - c_h + 2\sigma_{xz} - \sigma_{xx}\tan\phi + \sigma_{zz}\tan\phi}, \tag{20}$$

the failure criterion considering directional strength variation can then be written as:

$$f = \left(\sigma_{zz} - \sigma_{xx} - 2\sigma_{xz}\tan\phi\right)^2 + \left(c_v - c_h + 2\sigma_{xz} - \sigma_{xx}\tan\phi + \sigma_{zz}\tan\phi\right)^2 - \left(c_v + c_h - \sigma_{xx}\tan\phi - \sigma_{zz}\tan\phi\right)^2 \le 0. \tag{21}$$

5. Shakedown solution techniques

Based on Melan's shakedown theorem, the essence of shakedown analysis is to find the maximum admissible load within which a self-equilibrated residual stress field can be found so that the total stress state will not violate the yield criterion. Residual stresses are such that they can remain in the half-space after load application as a result of plastic deformation. In a three-dimensional half-space, there may be all the six components of residual stresses at a general material point. However, symmetry and other considerations impose some constrains. For the problem considered here, in which the material is homogeneous and cross-anisotropic with a vertical axis of symmetry, the resulting permanent deformation and therefore the residual stress field will be independent of the travel (x) direction. It has also been demonstrated by Yu [17] and Yu and Wang [18] that, under a moving three-dimensional Hertz load distribution, the most critical plane in the half-space is the central *xz* plane, defined by $y = 0$. On this plane, the only possible residual stress is the horizontal residual stress σ_{xx}^r, because the self-equilibrium and boundary conditions eliminate the possibility of residual shear stress σ_{xz}^r and residual vertical stress σ_{zz}^r. Therefore, the total stress field owing to a moving Hertz load distribution for an element on the $y = 0$ plane at any given moment can be defined as the sum of elastic stresses and residual stresses:

$$\sigma_{xx} = \lambda\sigma_{xx}^e + \sigma_{xx}^r \tag{22}$$

$$\sigma_{zz} = \lambda\sigma_{zz}^e \tag{23}$$

$$\sigma_{xz} = \lambda\sigma_{xz}^e \tag{24}$$

where λ is a dimensionless load parameter and σ_{ij}^e is the elastic stress field due to unit pressure p_0.

In the *y*-direction, a non-zero residual stress σ_{yy}^r may well exist, thus the total stress normal to the $y = 0$ plane is $\sigma_{yy} = \lambda\sigma_{yy}^e + \sigma_{yy}^r$. Since σ_{yy}^r is an arbitrary function of depth *z*, it can be chosen so that σ_{yy} is always the intermediate principle stress. In other words, the major and minor principle stresses are always on the $y = 0$ plane.

If the generalised, anisotropic Mohr-Coulomb yield criterion Eq. 21 is utilised to describe the material yield condition and σ_{yy} is the intermediate stress, Eq. 22 – Eq. 24 then are substituted to the yield criterion Eq. 21 to satisfy the requirement of Melan's shakedown theorem and this gives:

$$\begin{aligned} f = &\left(\lambda\sigma_{zz}^e - \lambda\sigma_{xx}^e - \sigma_{xx}^r - 2\lambda\sigma_{xz}^e \tan\phi\right)^2 + \left(c_v - c_h + 2\lambda\sigma_{xz}^e - \lambda\sigma_{xx}^e \tan\phi - \sigma_{xx}^r \tan\phi + \lambda\sigma_{zz}^e \tan\phi\right)^2 \\ &- \left(c_v + c_h - \lambda\sigma_{xx}^e \tan\phi - \sigma_{xx}^r \tan\phi - \lambda\sigma_{zz}^e \tan\phi\right)^2 \le 0, \end{aligned} \tag{25}$$

The above shakedown condition can be rewritten as follows:

$$f = \left(\sigma_{xx}^r + \mathrm{M}\right)^2 + \mathrm{N} + \mathrm{P} \le 0 \tag{26}$$

where σ_{xx}^{r} is self-equilibrated,

$$\mathrm{M} = \lambda\sigma_{xx}^{e} - \lambda\sigma_{zz}^{e} + 2\left(c_h - \lambda\sigma_{zz}^{e}\tan\phi\right)\tan\phi ,$$

$$\mathrm{N} = 4\left(\tan^2\phi + 1\right)\left[\left(\lambda\sigma_{xz}^{e}\right)^2 - \left(c_h - \lambda\sigma_{zz}^{e}\tan\phi\right)^2\right],$$

$$\mathrm{P} = 4\left(c_v - c_h\right)\left[\lambda\sigma_{xz}^{e} - \left(c_h - \lambda\sigma_{zz}^{e}\tan\phi\right)\right].$$

It should be noted that if c_v equals to c_h, then P is zero and Eq. 26 becomes equivalent to the shakedown condition of Yu and Wang [18] for the special case of isotropic materials.

In order to satisfy Eq. 26, one condition must be met:

$$\mathrm{N} + \mathrm{P} \le 0 \tag{27}$$

The above condition Eq. 27 can be rewritten as:

$$\mathrm{A} \times \mathrm{B} \le 0 \tag{28}$$

with

$$\mathrm{A} = \lambda\sigma_{xz}^{e} - \left(c_h - \lambda\sigma_{zz}^{e}\tan\phi\right),$$

$$\mathrm{B} = \left(\tan^2\phi + 1\right)\left[\lambda\sigma_{xz}^{e} + \left(c_h - \lambda\sigma_{zz}^{e}\tan\phi\right)\right] + c_v - c_h .$$

Table 1 summarises conditions of λ in order to satisfy Eq. 28, where

$$a = \sigma_{zz}^{e}\tan\phi + \sigma_{xz}^{e} , \tag{29}$$

$$b = \left(\sigma_{zz}^{e}\tan\phi - \sigma_{xz}^{e}\right)\frac{1+\tan^2\phi}{c_v / c_h + \tan^2\phi} . \tag{30}$$

At any point (x, y, z) in the half-space, a and b can be either positive or negative subject to elastic stresses at that point. For different combination of signs of a and b, there are different conditions for the load parameter λ in order to satisfy Eq. 28. Since each point in the half-space give one condition for λ, the overall shakedown condition for the half-space must be the intersection of all conditions, so that:

$$\lambda \le \min\left[\min_{case1}\left(\frac{c_h}{a}\right), \min_{case2}\left(\frac{c_h}{b}\right), \min_{case3}\left(\min\left[\frac{c_h}{a}, \frac{c_h}{b}\right]\right)\right]. \tag{31}$$

The above condition can be rewritten as:

$$\lambda \le \frac{c_h}{\max\left[\max_{case1}(a), \max_{case2}(b), \max_{case3}(a,b)\right]}, \tag{32}$$

By searching through every location in the half-space for the maximum value of $\left[\max_{case1}(a), \max_{case2}(b), \max_{case3}(a,b)\right]$, this condition can provide a necessary shakedown limit λ_{sd}, defined by:

$$\lambda_{sd} = \frac{c_h}{\max\left[\max_{case1}(a), \max_{case2}(b), \max_{case3}(a,b)\right]}. \tag{33}$$

Eq. 33 does not impose self-equilibrium condition of residual stress and therefore it provides a maximum boundary to the rigorous lower-bound shakedown limit. It is quite difficult to obtain the lower-bound shakedown limit without the known residual stress. However, Eq. 26 and the self-equilibrium condition impose some constrains on the residual stress field:

(1) Eq. 26 requires that at any point i in the half-space, the residual stress σ_{xx}^r must be between two roots of $f = 0$:

$$-\mathrm{M}_i - \sqrt{-\mathrm{N}_i - \mathrm{P}_i} \le \sigma_{xx}^r \le -\mathrm{M}_i + \sqrt{-\mathrm{N}_i - \mathrm{P}_i}, \tag{34}$$

where $-\mathrm{N}_i - \mathrm{P}_i$ must be non-negative if the necessary shakedown condition Eq. 32 is satisfied.

(2) The self-equilibrium condition requires that the residual stress σ_{xx}^r at any specific depth $z = j$ must be unique. Therefore, the possible residual stress at depth $z = j$ must be within the following criterion:

$$\max_{z=j}(-\mathrm{M}_i - \sqrt{-\mathrm{N}_i - \mathrm{P}_i}) \le \sigma_{xx}^r \le \min_{z=j}(-\mathrm{M}_i + \sqrt{-\mathrm{N}_i - \mathrm{P}_i}), \tag{35}$$

where $\sigma_{xx}^{r} = \min_{z=j}(-\mathrm{M}_i + \sqrt{-\mathrm{N}_i - \mathrm{P}_i})$ (referred to as 'minimum larger root') and $\sigma_{xx}^{r} = \max_{z=j}(-\mathrm{M}_i - \sqrt{-\mathrm{N}_i - \mathrm{P}_i})$ (referred to as 'maximum smaller root') are defined as critical residual stresses.

Given a load parameter λ equal or less than the shakedown limit, if the critical residual stress (either the minimum larger root or the maximum smaller root) is substituted into Eq. 26, it will lead to $\max_{z=j}(f) = 0$. However, when λ is larger than the shakedown limit, $\max_{z=j}(f)$ will be larger than zero. This is because when λ is above the shakedown limit, it is impossible to find a common residual stress that makes $f \le 0$ at all points at the same depth. The present shakedown problem now can be written as a mathematical formulation:

$$\text{maximise } \lambda,$$
$$\text{subject to } \begin{cases} f\left(\sigma_{xx}^{r}\left(\lambda\sigma^{e}\right), \lambda\sigma^{e}\right) \le 0, \\ \sigma_{xx}^{r}\left(\lambda\sigma^{e}\right) = \min_{z=j}(-\mathrm{M}_i + \sqrt{-\mathrm{N}_i - \mathrm{P}_i}) \text{ or } \sigma_{xx}^{r}\left(\lambda\sigma^{e}\right) = \max_{z=j}(-\mathrm{M}_i - \sqrt{-\mathrm{N}_i - \mathrm{P}_i}). \end{cases} \tag{36}$$

Eq. 36 can be reduced to the following expression with only one variable λ when the load form and the materials are determined:

$$\text{maximise } \lambda,$$
$$\text{subject to } f\left(\lambda\right) \le 0. \tag{37}$$

By using the elastic stress solutions Eq. 7 – Eq. 14, the maximum load parameter that makes $f(\lambda) \le 0$ at all points in the half-space is the rigorous lower-bound shakedown limit $\lambda_{sd}^{'}$ for the present anisotropic problem.

6. Numerical procedure and results

In this section, a procedure is suggested first to find the maximum load parameter for Eq. 36. This and elastic stress solutions have been programmed into FORTRAN. The elastic stress fields have been verified by comparing with finite element results using ABAQUS. Results are presented and discussed first for soils with elastic anisotropy only, and then for cases with plastic anisotropy.

6.1 Shakedown solution procedure

A simple procedure to solve Eq. 36 and obtain the lower-bound shakedown limit $\lambda_{sd}^{'}$ is outlined in Figure 3. First, using the necessary shakedown limit λ_{sd}, possible residual stresses $-\mathrm{M}_i+\sqrt{-\mathrm{N}_i-\mathrm{P}_i}$ and $-\mathrm{M}_i-\sqrt{-\mathrm{N}_i-\mathrm{P}_i}$ are calculated for each point i in the half-space. In numerical applications, the points were chosen with $0.01a$ intervals in each axis direction (x-direction, y-direction, z-direction) in a Cartesian coordinate system. Then, a critical residual stress field is obtained by calculating either the minimum larger root or the maximum smaller root at each depth. This step reduces the residual stress field as a function of depth z. Shakedown condition under this load parameter can be checked by substituting λ_{sd} and the critical residual stress field into Eq. 31. If the maximum value of f among all points is found to be very close to 0 (said 1e-3 here), the present lower-bound shakedown solution $\lambda_{sd}^{'}$ coincides with the necessary shakedown condition λ_{sd}. Otherwise, if $\max(f)$ is larger than 1e-3, a smaller load parameter is required. In the latter case, the problem becomes how to determine the maximum permissible load parameter $\lambda_{sd}^{'}$ at which the sum of corresponding elastic stresses and critical residual stresses fulfils the generalised Mohr Coulomb yield condition at every location in the half-space. Noticing that the load parameters have to lie between λ_{sd} and 0, a method of bisection is utilised to find the optimum shakedown limit efficiently. It was also found in the numerical practices that a very small change of load parameter λ_3 (said 1e-3) around the lower-bound shakedown limit results in a significant change of max(f), from 1e-7 to 1e-3 and consequently the condition 1e-4 ≤ max(f) ≤ 1e-3 is able to provide an accurate shakedown limit. At the shakedown load limit, the point providing the maximum value of f can be identified as the critical point.

Finally, when the load does not exceed the shakedown limit, the residual stress field itself calculated through the present procedure should satisfy the yield condition inherently (i.e. $f\left(\sigma_{xx}^{r}\left(\lambda_{sd}^{'}\sigma^{e}\right)\right)\leq 0$) once the chosen boundary is large enough. This is because when far-off points are taken into account during calculation, elastic stresses at those points are negligible so that only the residual stress holds their f values which then contribute to $\max(f)$. This can be checked by substituting the critical residual stress only into the condition Eq. 31.

6.2 Results and discussion

In the following results, the lower-bound shakedown limit obtained through this program is defined in terms of the maximum pressure p_0 in a dimensionless form: $k'_{\max} = \lambda'_{sd} p_0 / c_h$. The load limit obtained by the necessary shakedown condition Eq. 33 is also defined in an analogous form: $k_{\max} = \lambda_{sd} p_0 / c_h$.

6.2.1 Special case - isotropic half-space

First, in order to verify the validity of the proposed shakedown solution, the half-space is assumed to be isotropic so that the numerical result can be compared with others. The numerical result of the shakedown limit of a half-space under moving pressure is presented in Figure 4, where the variation of material friction angle ϕ is also considered. The present shakedown solutions are close to the numerical lower-bounds obtained by Shiau [38] using finite elements and nonlinear programming techniques. It also shows that the shakedown limits increase significantly with the rising of the friction angle.

6.2.2 Effect of elastic cross-anisotropic parameters

Analyses were then presented in consideration of elastic anisotropy only. As mentioned before, the elastic stress fields for a cross-anisotropic material are dependent on five elastic parameters, and here the following parameters were used: E_h, E_v/E_h, G_{vh}/G_h, υ_h and υ_{vh}. Table 2 compares the theoretical shakedown limits based on the isotropic assumption and those obtained using anisotropic parameters. Those anisotropic elastic parameters were calculated from real test data of Graham and Houlsby [21] for Winnipeg Clay. It demonstrates that the use of conventional isotropic assumption overestimates the shakedown limit by as much as 20%. As a result, ignoring elastic soil anisotropy in shakedown analysis may lead to unsafe pavement design.

Further investigations show that for the problem of a homogeneous half-space, the shakedown limit is not influenced by Young's modulus in a particular direction (i.e. E_h or E_v), but affected by Young's modulus ratio E_v/E_h. This agrees with shakedown solutions in an isotropic homogeneous half-space which do not vary with Young's modulus. In addition, the change of Poisson's ratio only leads to a slightly variation of shakedown limits as presented in Figure 5.

Figure 6 and Figure 7 show the variations of shakedown limit with respect to frictional coefficient μ for different values of Young's modulus ratio E_v/E_h and shear modulus ratio

G_{vh}/G_h. In these figures, the trend observed for the anisotropic solutions (i.e. $E_v/E_h \neq 1$ or $G_{vh}/G_h \neq 1$) follows that for the isotropic solutions where the shakedown limit decreases with increasing frictional coefficient μ. Also, it is accompanied by the move of critical point location, from a point below the surface (referred to as 'subsurface failure') towards a point on the surface (referred to as 'surface failure'). The turning point splitting subsurface failure cases and surface failure cases tends to occur at a larger value of μ for a smaller value of E_v/E_h or for a larger value of G_{vh}/G_h. This implies that subsurface failure is more likely to occur when $E_v < E_h$ and $G_{vh} > G_h$. When subsurface failure is critical, the shakedown limit can be raised by increasing E_v/E_h or decreasing G_{vh}/G_h until it reaches a peak value. When surface failure is critical, shakedown limit can be increased by rising G_{vh}/G_h, especially in the case of cohesive-frictional material (Figure 7b).

It is instructive to reveal the interactive effect of E_v/E_h and G_{vh}/G_h on the shakedown limit, as shown in Figure 8. The results are presented in a logarithmic scale. When the frictional coefficient μ is zero, failure always initiates below the surface (i.e. subsurface failure), and the shakedown limit changes more quickly with E_v/E_h than with G_{vh}/G_h until a peak value is reached. In these figures, the peak value is around 5 for $\phi = 0°$ and around 22 for $\phi = 30°$. When the frictional coefficient $\mu = 0.5$, the critical points mostly lie on the surface (i.e. surface failure) and the change of shakedown limit is dominated by the variation of G_{vh}/G_h, not E_v/E_h, except those at the lower-right corner of which the shakedown limit is controlled by subsurface critical points. A maximum value $k'_{\max} = 2$ is also observed for the case $\phi = 0°$. These results implies that when elastic anisotropy is taken into account, the shakedown solutions for cohesive-frictional materials under a three-dimensional Hertz load tend to be controlled by E_v/E_h for subsurface failure cases but by G_{vh}/G_h for surface failure cases.

6.2.3 Effect of plastic anisotropy

Figure 9 presents the shakedown limit against frictional coefficient μ for different values of cohesion ratio c_v/c_h, while the soil friction angle ϕ is taken as 0°, 15°, 30°, 45° respectively. Variation of shakedown solutions with respect to c_v/c_h is also plotted in Figure 10. Some features can be drawn as follows:

(1) When c_v/c_h is smaller than 1, the shakedown solution reduces as the frictional coefficient increases. This trend follows that for the isotropic solutions (i.e. $c_v/c_h = 1$). When c_v/c_h is larger than 1, there exists a peak value of shakedown solutions giving an optimum

frictional coefficient μ (> 0). This is different from the isotropic solutions of which the value is always maximum when $\mu = 0$ (i.e. normal load only).

(2) The rise of c_v/c_h does not always lead to an increase of the shakedown limit which is defined as $k'_{\max} = \lambda'_{sd} p_0 / c_h$. As shown in Figure 10, the shakedown limit rises proportionally with increasing c_v/c_h when the lower-bound shakedown limit $k'_{\max}$ equals the necessary shakedown condition $k_{\max}$ and its value is controlled by $1/b$ (refer to Eq. 30). However, this growth is not always proportional, such as those in Figure 10c, 10d where $k_{\max}$ is smaller than $k'_{\max}$. If c_v/c_h is large enough, the shakedown limit will finally reach a maximum value which is controlled by $1/a$ (refer to Eq. 29).

(3) Results in Figure 9 are divided into surface failure cases and subsurface failure cases by a dash line and a dot line. The dot line represents subsurface failure cases of which value is controlled by $1/a$. On the left hand side of the dash line, the critical point initiates below the surface and the lower-bound shakedown limit is controlled by $1/b$. On the right hand side, the shakedown limit is controlled by critical point on the surface.

(4) Surface failure is most likely to occur when c_v/c_h is around 2. When c_v/c_h is either very large (e.g. $c_v/c_h = 10$) or very small (e.g. $c_v/c_h = 0.1$), failure tends to initiate below surface.

(5) As the friction angle increases, the dot line becomes steeper and the dash line moves towards left. This means surface failure tends to occur at a higher value of friction angle in anisotropic materials.

6.2.4 Effect of combined elastic and plastic anisotropies

Previous analyses examined the influences of elastic and plastic anisotropies independently. However, the elastic and plastic parameters in a real soil are somewhat related [30]. For example, soils compacted more in the horizontal direction could have $E_v > E_h$ as well as $c_v > c_h$. Table 3 compares isotropic shakedown solutions with those of two anisotropic cases which are closer to real situations:

(i) $E_v/E_h = 0.5$, $G_{vh}/G_h = 0.7$, $\upsilon_h = 0.15$, $\upsilon_{vh} = 0.22$, $c_v/c_h = 0.8$;

(ii) $E_v/E_h = 1.5$, $G_{vh}/G_h = 1.2$, $\upsilon_h = 0.15$, $\upsilon_{vh} = 0.12$, $c_v/c_h = 1.2$.

It is clear that the isotropic solutions are larger than the shakedown solutions of case (i) by as much as 38%, while they are smaller than the shakedown solutions of case (ii) by as much as

42%. Therefore both elastic and plastic anisotropies should be taken into account in calculating shakedown limits of soil half-space under moving surface loads.

7. Concluding remarks

Based on Melan's shakedown theorem, this paper develops lower-bound shakedown solutions for an anisotropic cohesive-frictional half-space under three-dimensional surface loads. Apart from cross-anisotropic elastic stress fields, a direction-dependent cohesion was used to generalise the Mohr-Coulomb criterion so that plastic anisotropy is also considered. Given a self-equilibrated critical residual stress field, the shakedown problem is reduced to a function of load parameter, which can be solved by a proposed numerical procedure. The anisotropic shakedown solutions can be reduced back to the solutions of Yu and Wang (2012) for isotropic materials.

Although five parameters define the cross-anisotropic elastic behaviour, it was found that lower-bound shakedown solutions for the present problem are mainly affected by the Young's modulus ratio E_v/E_h and the shear modulus ratio G_{vh}/G_h. Moreover, when subsurface failure is critical, the shakedown limits are dominated by the Young's modulus ratio; when surface failure is critical, the shakedown limits are dominated by the shear modulus ratio.

With the rise of cohesion ratio c_v/c_h, the anisotropic shakedown limits are trending upwards (the increase rate is equal or smaller than that of c_v/c_h); however, it flattens out when a maximum value is reached. In general, the anisotropic shakedown limits are identical to the necessary shakedown condition for subsurface failure cases (i.e. rolling with limited sliding); otherwise, the shakedown limits are controlled by surface critical points (i.e. rolling with significant sliding). In addition, subsurface failure tends to occur when c_v/c_h is either very large or very small. For any cases of $c_v/c_h > 1$, a peak point exists when shakedown limit varying with frictional coefficient μ (from 0 to 1). This is different from isotropic solutions which are always largest at $\mu = 0$ (i.e. normal load only).

Acknowledgements

The work reported in this paper forms part of an on-going research programme at the Nottingham Centre for Geomechanics (NCG) on shakedown theory and its application to the design of pavement and railway foundations. The Authors wish to thank the UK's Engineering and Physical Science Research Council (EPSRC) and the University of Nottingham for their financial support.

References

1. Yu HS. *Plasticity and geotechnics*. Springer, 2006.
2. Brown SF, Yu HS, Juspi S, Wang J. Validation experiments for lower bound shakedown theory applied to layered pavement systems. *Géotechnique* 2012; **62**: 923-932.
3. Wang J, Yu HS. Shakedown and residual stresses in cohesive-frictional half-space under moving surface loads. *Geomechanics and Geoengineering: An International Journal* 2013; **8**, 1-14.
4. Sharp RW, Booker JR. Shakedown of pavements under moving surface loads. *Journal of Transportation Engineering, ASCE* 1984; **110**: 1-14.
5. Yu HS, Hossain MZ. Lower bound shakedown analysis of layered pavements using discontinuous stress fields. *Computer Methods in Applied Mechanics and Engineering* 1998; **167**: 209-222.
6. Ravindra PS, Small JC. Shakedown analysis of road pavements. In: *The 12th International Conference of International Association for Computer Methods and Advances in Geomechanics*, 2008; Goa, India. 4432-4438.
7. Koiter WT. General theorems for elastic-plastic solids. In: *Progress in solid mechanics*, Sneddon IN, Hill R (eds). Amsterdam: North Holland, 1960; 165-221.
8. Melan E. Der Spannungszustand eines Hencky-Mises'schen Kontinuums bei veränderlicher Belastung. *Sitzungberichte der Ak. Wissenschaften Wien (Ser. 2A)* 1938; **147**: 73.
9. Ponter ARS, Hearle AD, Johnson KL. Application of the kinematical shakedown theorem to rolling and sliding point contacts. *Journal of the Mechanics and Physics of Solids* 1985; **33**: 339-362.
10. Collins IF, Cliffe PF. Shakedown in frictional materials under moving surface loads. *International Journal for Numerical and Analytical Methods in Geomechanics* 1987; **11**: 409-420.
11. Boulbibane M, Ponter ARS. Extension of the linear matching method to geotechnical problems. *Computer Methods in Applied Mechanics and Engineering* 2005; **194**: 4633-4650.
12. Boulbibane M, Collins IF, Weichert D, Raad L. Shakedown analysis of anisotropic asphalt concrete pavements with clay subgrade. *Canadian Geotechnical Journal* 2000; **37**: 882-889.

13. Raad L, Weichert D, Najm W. Stability of multilayer systems under repeated loads. *Transportation Research Record* 1988; **1207**: 181-186.
14. Shiau SH, Yu HS. Load and displacement prediction for shakedown analysis of layered pavements. *Transportation Research Record* 2000; **1730**: 117-124.
15. Nguyen AD, Hachemi A, Weichert D. Application of the interior-point method to shakedown analysis of pavements. *International Journal for Numerical Methods in Engineering* 2008; **75**: 414-439.
16. Krabbenhøft K, Lyamin AV, Sloan SW. Shakedown of a cohesive-frictional half-space subjected to rolling and sliding contact. *International Journal of Solids and Structures* 2007; **44**: 3998-4008.
17. Yu HS. Three-dimensional analytical solutions for shakedown of cohesive-frictional materials under moving surface loads. *Proceedings of the Royal Society A: Mathematical, Physical and Engineering Science* 2005; **461**: 1951-1964.
18. Yu HS, Wang J. Three-dimensional shakedown solutions for cohesive-frictional materials under moving surface loads. *International Journal of Solids and Structures* 2012; **49**: 3797-3807.
19. Oda M, Koishikawa I, Higuchi T. Experimental study of anisotropic shear strength of sand by plane strain test. *Soils and Foundations* 1978; **18**: 25-38.
20. Arthur JRF, Menzies BK. Inherent anisotropy in a sand. *Géotechnique* 1972; **22**: 115-128.
21. Graham J, Houlsby GT. Anisotropic elasticity of a natural clay. *Géotechnique* 1983; **33**: 165-180.
22. Oda M, Koishikawa I. Effect of strength anisotropy on bearing capacity of shallow footing in a dense sand. *Soils and Foundations* 1979; **19**: 15-28.
23. Azami A, Pietruszczak S, Guo P. Bearing capacity of shallow foundations in transversely isotropic granular media. *International Journal for Numerical and Analytical Methods in Geomechanics* 2010; **34**: 771-793.
24. Yu HS, Sloan SW. Limit analysis of anisotropic soils using finite elements and linear programming. *Mechanics Research Communications* 1994; **21**: 545-554.
25. Lings ML, Penningtonf DS, Nash DFT. Anisotropic stiffness parameters and their measurement in a stiff natural clay. *Géotechnique* 2000; **50**: 109-125.
26. Yu S, Dakoulas P. General stress-dependent elastic moduli for cross-anisotropic soils. *Journal of Geotechnical Engineering* 1993; **119**: 1568-1586.

27. Yimsiri S, Soga K. Cross-anisotropic elastic parameters of two natural stiff clays. *Géotechnique* 2011; **61**: 809-814.

28. Hoque E, Tatsuoka F, Sato T. Measuring anisotropic elastic properties of sand using a large triaxial specimen. *Geotechnical Testing Journal* 1996; **19**: 411-420.

29. Kuwano R, Jardine RJ. On the applicability of cross-anisotropic elasticity to granular materials at very small strains. *Géotechnique* 2002; **52**: 727-749.

30. Jiang GL, Tatsuoka F, Flora A, Koseki J. Inherent and stress-state-induced anisotropy in very small strain stiffness of a sandy gravel. *Géotechnique* 1997; **47**: 509-521.

31. Guo P. Modified direct shear test for anisotropic strength of sand. *Journal of Geotechnical and Geoenvironmental Engineering* 2008; **134**: 1311-1318.

32. Lo KY. Stability of Slopes in Anistropic Soils. *Journal of Soil Mechanics and Foundations Division, ASCE* 1965; **91**: 85-106.

33. Wong RKS, Arthur JRF. Induced and inherent anisotropy in sand. *Géotechnique* 1985; **35**: 471-481.

34. Kurukulasuriya LC, Oda M, Kazama H. Anisotropy of undrained shear strength of an over-consolidated soil by triaxial and plane strain tests. *Soils and Foundations* 1999; **39**: 21-30.

35. Lade PV. Modeling failure in cross-anisotropic frictional materials. *International Journal of Solids and Structures* 2007; **44**: 5146-5162.

36. Gao Z, Zhao J, Yao Y. A generalized anisotropic failure criterion for geomaterials. *International Journal of Solids and Structures* 2010; **47**: 3166-3185.

37. Hanson MT. The elastic field for spherical Hertzian contact including sliding friction for transverse isotropy. *Journal of Tribology* 1992; **114**: 606-611.

38. Shiau SH *Numerical methods for shakedown analysis of pavements under moving surface loads*. Ph.D. thesis, The University of Newcastle, Australia.

Table 1. Necessary shakedown conditions

case	a	b	possible conditions from Eq. 28	summary of possible conditions	conditions for each case
1	+	−	$\lambda \le \frac{c_h}{a} \cap \lambda \ge \frac{c_h}{b}$	$0 \le \lambda \le \frac{c_h}{a}$	$0 \le \lambda \le \frac{c_h}{a}$
			or $\lambda \ge \frac{c_h}{a} \cap \lambda \le \frac{c_h}{b}$	NA	
2	−	+	$\lambda \ge \frac{c_h}{a} \cap \lambda \le \frac{c_h}{b}$	$0 \le \lambda \le \frac{c_h}{b}$	$0 \le \lambda \le \frac{c_h}{b}$
			or $\lambda \le \frac{c_h}{a} \cap \lambda \ge \frac{c_h}{b}$	NA	
3	+	+	$\lambda \le \frac{c_h}{a} \cap \lambda \le \frac{c_h}{b}$	$\lambda \le \min\left[\frac{c_h}{a}, \frac{c_h}{b}\right]$	$\lambda \le \min\left[\frac{c_h}{a}, \frac{c_h}{b}\right]$
			or $\lambda \ge \frac{c_h}{a} \cap \lambda \ge \frac{c_h}{b}$	$\lambda \ge \max\left[\frac{c_h}{a}, \frac{c_h}{b}\right]$	
4	−	−	$\lambda \ge \frac{c_h}{a} \cap \lambda \ge \frac{c_h}{b}$	$\lambda \ge 0$	$\lambda \ge 0$
			or $\lambda \le \frac{c_h}{a} \cap \lambda \le \frac{c_h}{b}$	NA	

(Note: $\lambda \ge 0$ is prerequisite; NA means not available)

Table 2. Effect of elastic anisotropy on shakedown limit of Winnipeg Clay

case	E_h (MPa)	E_v/E_h	G_{vh}/G_h	υ_h	υ_{vh}	Shakedown limit	difference
1	9.35	0.53	0.73	0.17	0.23	*4.00*	-15%
2	6.96	0.41	0.64	0.08	0.12	*3.74*	-20%
3	7.67	0.52	0.72	0.17	0.23	*3.97*	-15%
4	5.76	0.76	0.87	0.23	0.27	*4.37*	-7%
isotropy						4.68	

Table 3. Comparison of isotropic and anisotropic shakedown solutions

case	μ	ϕ (°)	E_v/E_h	G_{vh}/G_h	υ_h	υ_{vh}	c_v/c_h	shakedown limit	difference
1	0	0	1	1	0.15	0.15	1	***4.68***	
2	0	0	0.5	0.7	0.15	0.22	0.8	*3.14*	*-33%*
3	0	0	2	1.4	0.15	0.11	1.2	*5.31*	*13%*
4	0	30	1	1	0.15	0.15	1	***13.47***	
5	0	30	0.5	0.7	0.15	0.22	0.8	*8.37*	*-38%*
6	0	30	2	1.4	0.15	0.11	1.2	*19.15*	*42%*
7	0.5	0	1	1	0.15	0.15	1	***2.00***	
8	0.5	0	0.5	0.7	0.15	0.22	0.8	*1.60*	*-20%*
9	0.5	0	2	1.4	0.15	0.11	1.2	*2.37*	*18%*
10	0.5	30	1	1	0.15	0.15	1	***2.93***	
11	0.5	30	0.5	0.7	0.15	0.22	0.8	*2.42*	*-17%*
12	0.5	30	2	1.4	0.15	0.11	1.2	*3.74*	*28%*

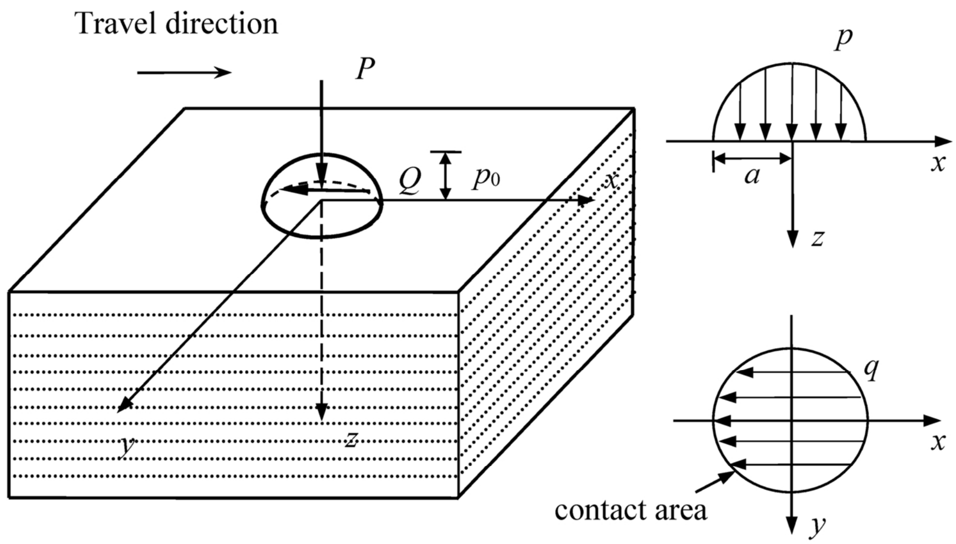

Figure 1. Cross-anisotropic soil half-space under moving three-dimensional loads
69x40mm (600 x 600 DPI)

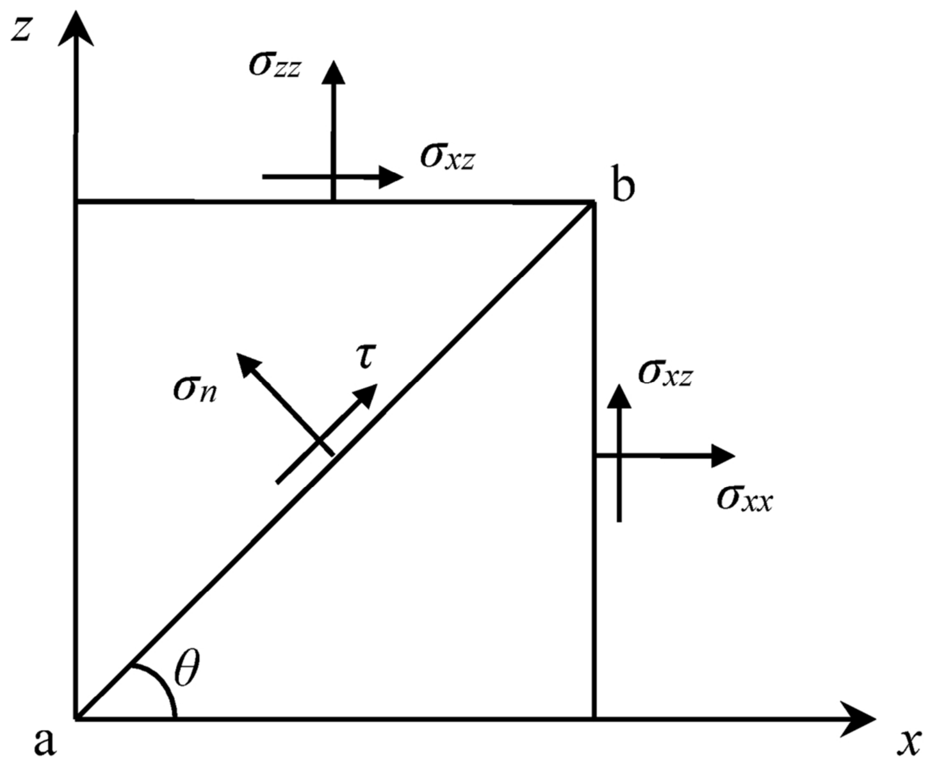

Figure 2. Stress transformation
49x41mm (600 x 600 DPI)

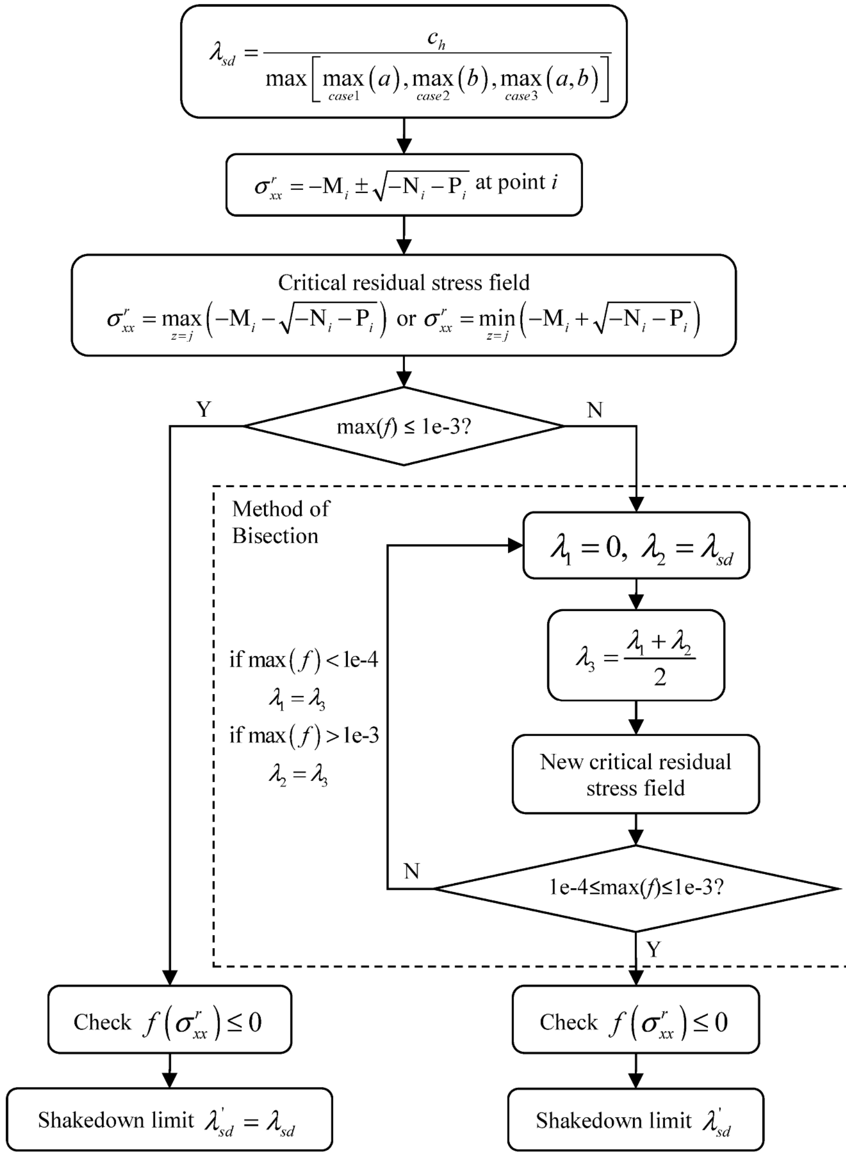

Figure 3. Program procedure
165x223mm (600 x 600 DPI)

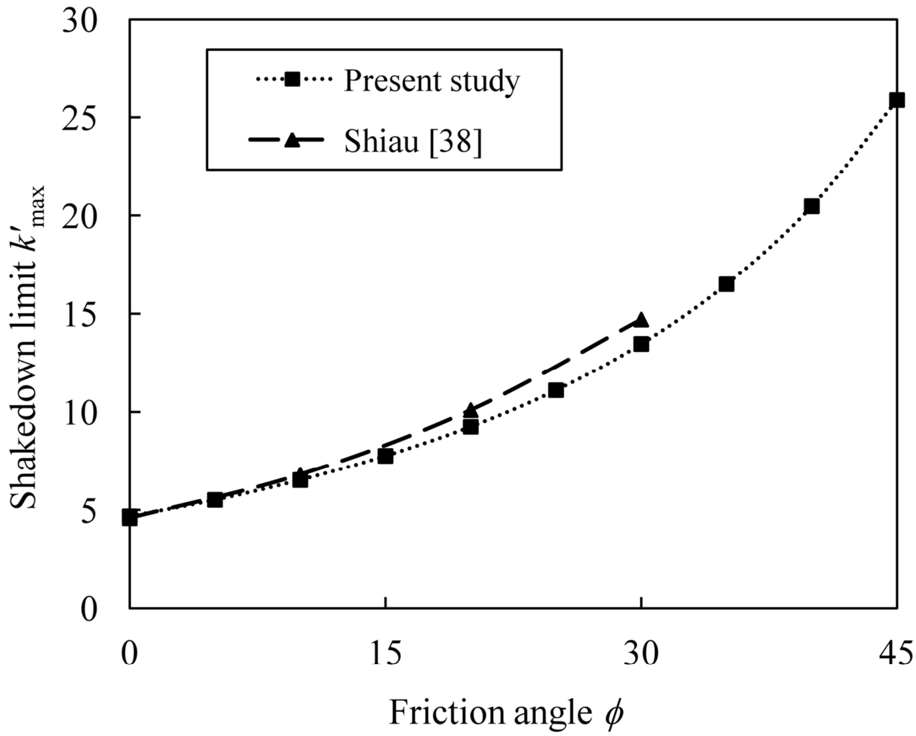

Figure 4. Comparison of shakedown limits for isotropic cohesive-frictional materials
82x65mm (600 x 600 DPI)

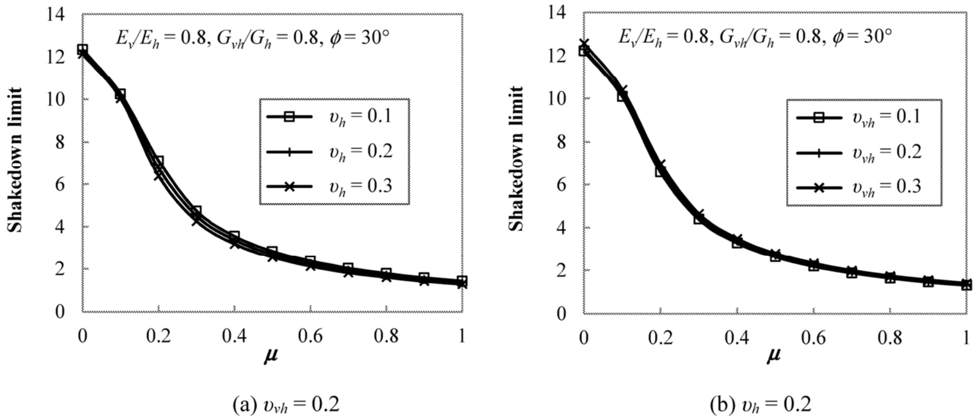

Figure 5. Variation of shakedown limit against frictional coefficient for different values of Poisson's ratio
69x31mm (600 x 600 DPI)

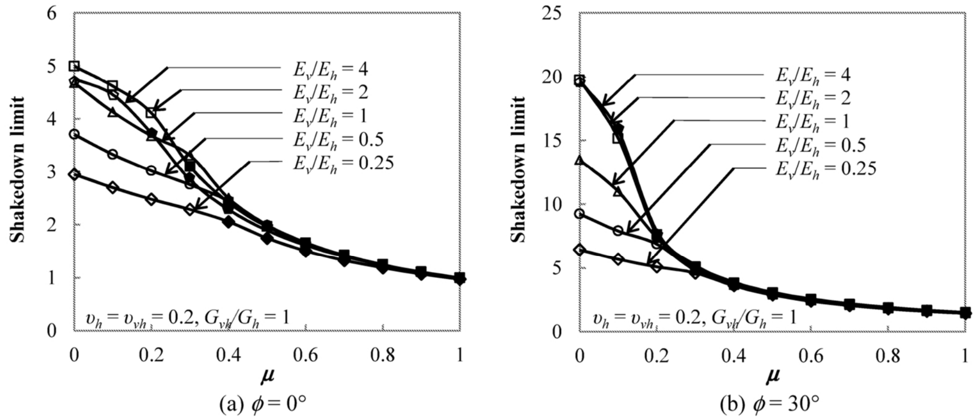

Figure 6. Variation of shakedown limit against frictional coefficient for different values of Young's modulus ratio (Hollow marker corresponds to subsurface failure; solid marker corresponds to surface failure)
68x30mm (600 x 600 DPI)

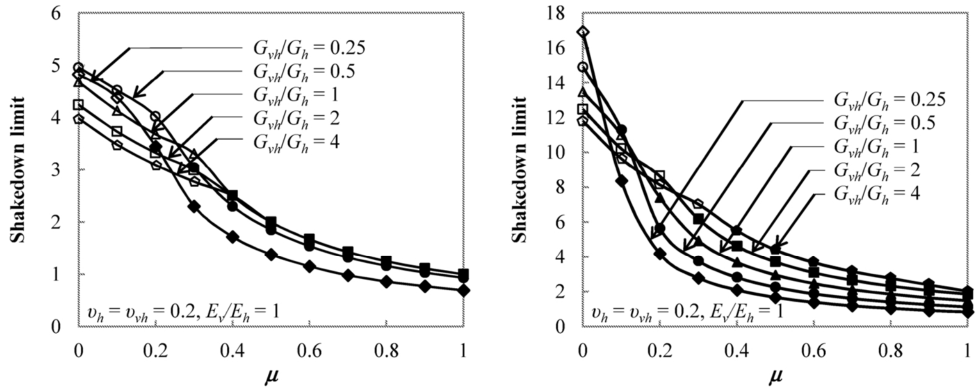

(a) $\phi = 0°$ (b) $\phi = 30°$

Figure 7. Variation of shakedown limit against frictional coefficient for different values of shear modulus ratio (Hollow marker corresponds to subsurface failure; solid marker corresponds to surface failure)
68x30mm (600 x 600 DPI)

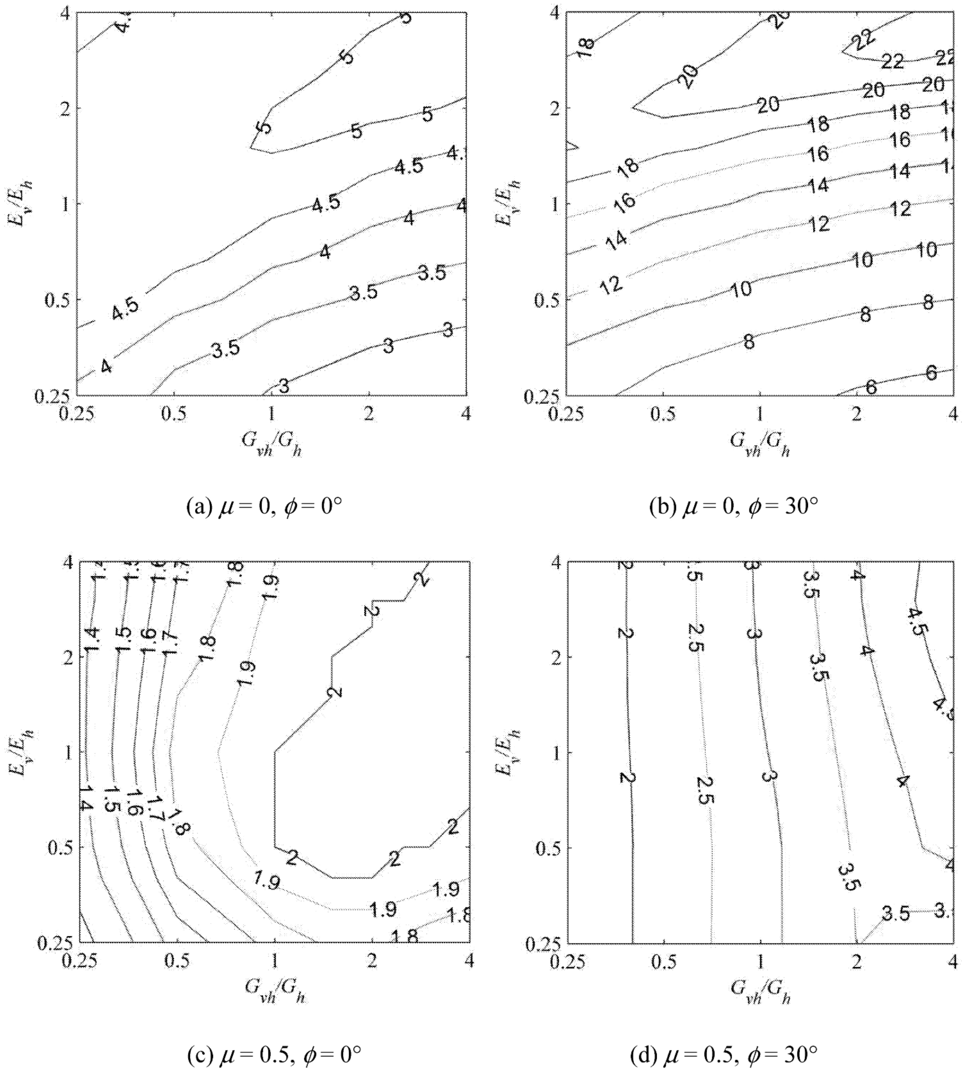

(a) $\mu = 0$, $\phi = 0°$

(b) $\mu = 0$, $\phi = 30°$

(c) $\mu = 0.5$, $\phi = 0°$

(d) $\mu = 0.5$, $\phi = 30°$

Figure 8. Contour plot of shakedown limits
176x193mm (600 x 600 DPI)

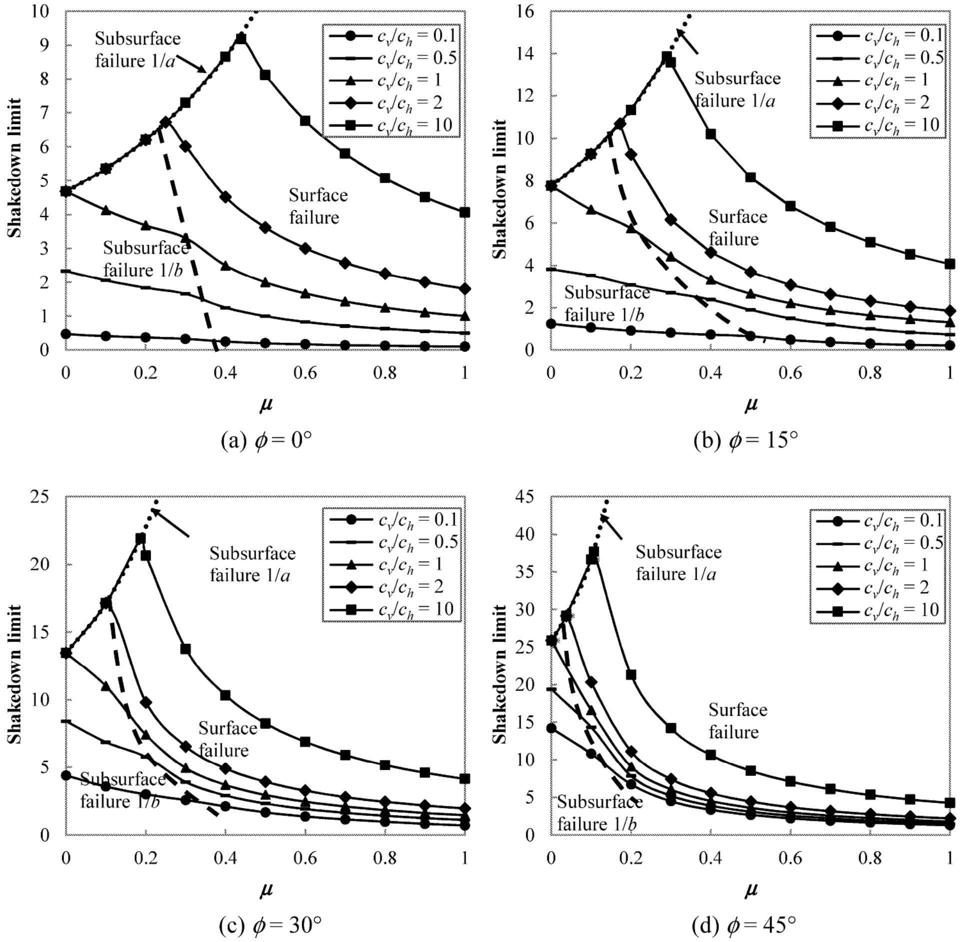

Figure 9. Variation of shakedown limit against frictional coefficient for different values of cohesion ratio (E_v/E_h=1, G_{vh}/G_h=1,v_h=v_{vh}=0.2)
158x153mm (600 x 600 DPI)

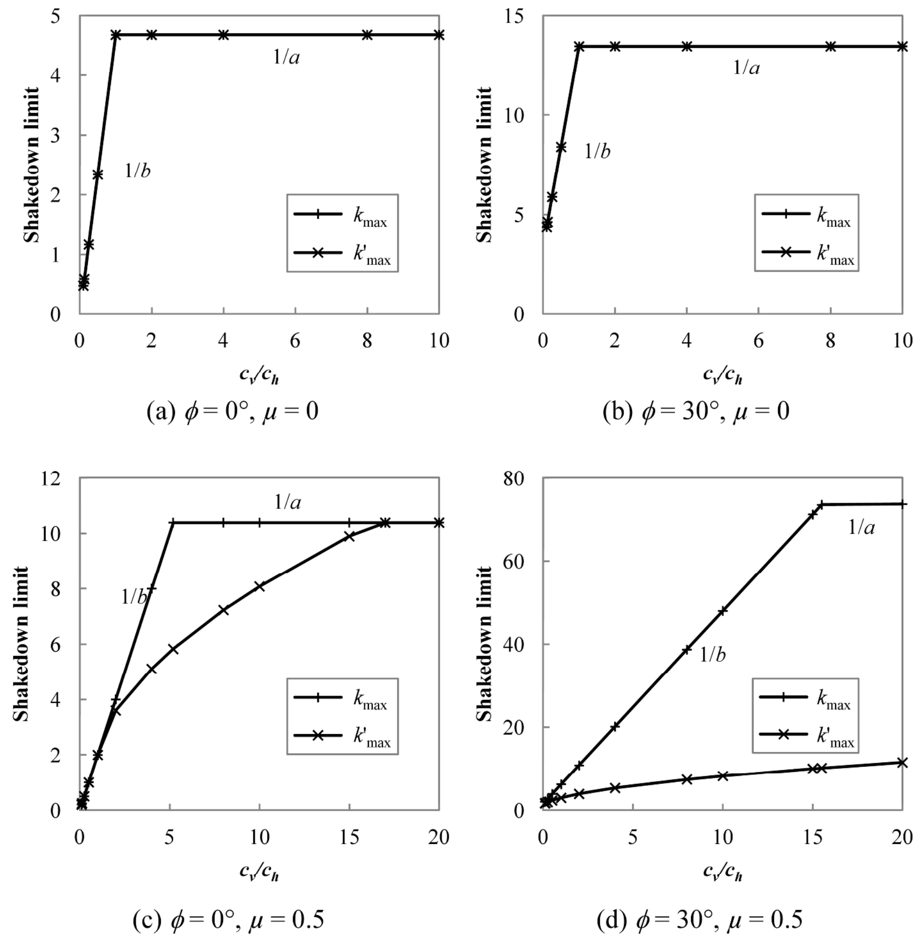

Figure 10. Variation of shakedown limit against cohesion ratio (E_v/E_h=1, G_{vh}/G_h=1,v_h=v_{vh}=0.2)
145x145mm (600 x 600 DPI)